



1 **Enhancement of Secondary Organic Aerosol Formation and its**

2 **Oxidation State by SO₂ during Photooxidation of 2-Methoxyphenol**

3 Changgeng Liu^{1,2,a}, Tianzeng Chen^{1,4,a}, Yongchun Liu^{1,4,5,*}, Jun Liu^{1,4}, Hong He^{1,3,4,*},

4 Peng Zhang^{1,4}

5 ¹State Key Joint Laboratory of Environment Simulation and Pollution Control,

6 Research Center for Eco-Environmental Sciences, Chinese Academy of Sciences,

7 Beijing 100085, China

8 ²School of Biological and Chemical Engineering, Panzhihua University, Panzhihua

9 617000, China

10 ³Center for Excellence in Regional Atmospheric Environment, Institute of Urban

11 Environment, Chinese Academy of Sciences, Xiamen 361021, China

12 ⁴University of Chinese Academy of Sciences, Beijing 100049, China

13 ⁵Beijing Advanced Innovation Center for Soft Matter Science and Engineering, Beijing

14 University of Chemical Technology, Beijing 100029, China

15 ^aThese authors contributed equally to this work and should be considered as co-first

16 authors

17 *Correspondence to:* Yongchun Liu (liuyc@buct.edu.cn) and Hong He

18 (honghe@rcees.ac.cn)



19 **Abstract.** 2-Methoxyphenol (guaiacol) is derived from the lignin pyrolysis and taken
20 as a potential tracer for wood smoke emissions. In this work, the effect of SO₂ at
21 atmospheric levels (0–56 ppb) on secondary organic aerosol (SOA) formation and its
22 oxidation state during guaiacol photooxidation was investigated in the presence of
23 various inorganic seed particles (NaCl and (NH₄)₂SO₄). Without SO₂ and seed particles,
24 SOA yields (9.46–26.37%) obtained at different guaiacol concentration
25 (138.83–2197.36 μg m⁻³) could be well expressed by a one-product model. The
26 presence of SO₂ resulted in enhancing SOA yield by 14.05–23.66%. With (NH₄)₂SO₄
27 and NaCl seed particles, SOA yield was enhanced by 23.06% and 29.57%, respectively,
28 which further increased significantly to 29.78–53.47% in the presence of SO₂,
29 suggesting that SO₂ and seed particles have a synergetic contribution to SOA formation.
30 It should be noted that SO₂ was found to be in favor of increasing the carbon oxidation
31 state (OS_C) of SOA, indicating that the functionalization reaction should be more
32 dominant than oligomerization reaction. In addition, the average N/C ratio of SOA was
33 0.037, which revealed that NO_x participated in the photooxidation process,
34 consequently leading to the formation of organic nitrates. The experimental results
35 demonstrate the importance of SO₂ on the formation processes of SOA and
36 organosulfates, and also are helpful to further understand SOA formation from the
37 atmospheric photooxidation of guaiacol and its subsequent impacts on air quality and
38 climate.



39 1 Introduction

40 Biomass burning is considered as one of the major sources of gas and particulate
41 pollutants in the atmosphere (Lauraguais et al., 2014b; Yang et al., 2016). Therefore, it
42 has significant adverse impacts on regional and global air quality (Bari and Kindzierski,
43 2016; Lelieveld et al., 2001), climate (Chen and Bond, 2010), and human health
44 (Naeher et al., 2007). The chemical species emitted by biomass burning is mainly
45 dependent on fuel source and combustion conditions (O'Neill et al., 2014). Natural
46 wood is composed of cellulose (40–50 wt.%), hemicelluloses (25–35 wt.%), and lignin
47 (18–35 wt.%) (Nolte et al., 2001). During the burning process, lignin pyrolysis could
48 result in the formation of methoxyphenols, mainly including guaiacol (2-
49 methoxyphenol), syringol (2,6-dimethoxyphenol), and their derivatives (Nolte et al.,
50 2001; Schauer et al., 2001). Due to the high emission rate of methoxyphenols
51 ($900\text{--}4200\text{ mg (kg of fuel)}^{-1}$), methoxyphenols are considered as the potential tracers
52 for wood burning (Hawthorne et al., 1989, 1992; Simoneit et al., 1993).

53 As a representative type of methoxyphenols, guaiacol mainly exists in the gas phase
54 and is widely found in the atmosphere (Schauer et al., 2001). Its emission factor of
55 wood burning is in the range of $172\text{--}279\text{ mg kg}^{-1}\text{ fuel}$ (Schauer et al., 2001). In recent
56 years, the reactivity of gas-phase guaiacol toward OH radicals (Coeur-Tourneur et al.,
57 2010a), NO₃ radicals (Lauraguais et al., 2016; Yang et al., 2016), chlorine atom
58 (Lauraguais et al., 2014a), and O₃ (El Zein et al., 2015) has been investigated,
59 suggesting that its degradation by OH radicals and NO₃ radicals might be predominant



60 in the atmosphere. Meanwhile, several studies have reported the significant SOA
61 formation from guaiacol oxidation by OH radicals (Ahmad et al., 2017; Lauraguais et
62 al., 2014b; Ofner et al., 2011; Sun et al., 2010; Yee et al., 2013). However, SOA
63 formation from the photooxidation of guaiacol in the presence of NO_x has not been
64 determined yet, even though it has been recently reported that the atmospheric level of
65 NO_x could reach up to close 200 ppb in the severely polluted climate in China (Li et al.,
66 2017).

67 Although many studies concentrated on the SOA production from the oxidation of
68 volatile organic compounds (VOCs), the reported SOA yields showed high variability
69 for a given precursor (Chu et al., 2016, 2017; Ge et al., 2017a; Lauraguais et al., 2012,
70 2014b; Ng et al., 2007; Sarrafzadeh et al., 2016; Yee et al., 2013). This variability is
71 mainly dependent on the numerous factors, e.g., pre-existing seed particles, SO₂ level,
72 NO_x level, humidity, and temperature. Two of the critical factors are the impacts of pre-
73 existing seed particles and SO₂ level on SOA formation (Chu et al., 2016, 2017; Ge et
74 al., 2017a). In addition, the atmospheric concentration of SO₂ could be up to close 200
75 ppb in the severely polluted atmosphere in China, and SOA from biomass burning and
76 sulfate formation could significantly contribute to severe haze pollution (Li et al., 2017).
77 During the transport process, smoke plumes from biomass burning would be inevitably
78 mixed with suspended particles (e.g., (NH₄)₂SO₄ particles), SO₂, and NO_x in the
79 atmosphere. However, the influences of these co-existed pollutants on the
80 transformation of guaiacol and its SOA formation are still unclear. For these reasons,



81 the aim of this work was to investigate the SOA formation from guaiacol
82 photooxidation in the presence of NO_x in a 30 m³ indoor smog chamber, as well as the
83 effect of SO₂ on SOA formation with various inorganic seed particles.

84 **2 Experimental section**

85 The photooxidation experiments were performed in a 30 m³ indoor smog chamber (4
86 m (high) × 2.5 m (wide) × 3 m (length)), which was built in a temperature-controlled
87 room located at the Research Center for Eco-Environment Sciences, Chinese Academy
88 of Sciences (RCEES-CAS). Its schematic structure is shown in Fig. S1. Briefly, 120
89 UV lamps (365 nm, Philips TL 60/10R) were taken as the light source with a NO₂
90 photolysis rate of 0.55 min⁻¹, which is comparable to the irradiation intensity at noon in
91 Beijing (Chou et al., 2011). A maglev fan installed at the bottom center of the smog
92 chamber was used to mix sufficiently the introduced gas species and seed particles.
93 Temperature and relative humidity (RH) in the chamber were (302 ± 1) K and (39 ±
94 1)%, respectively. Before each experiment, the chamber would be flushed by purified
95 dry zero air for ~36 h with a flow rate of 100 L min⁻¹ until the particle number
96 concentration in the chamber was lower than 20 cm⁻³.

97 Gas-phase guaiacol was firstly introduced into the chamber by purified dry zero air
98 flowing through the gently heated injector with a known volume of pure liquid guaiacol
99 until guaiacol fully vaporized. Its concentration in the chamber was online monitored
100 by a proton-transfer reaction time-of-flight mass spectrometer (PTR-QiToF-MS)
101 (Ionicon Analytik GmbH), and was calibrated by a commercial permeation tube (VICI



102 AG INTERNATIONAL Valco Instruments Co., Inc.). When guaiacol concentration
103 was stable, NO and SO₂ were introduced into the chamber by a gas controller using
104 purified dry zero air as the carrier gas. Their concentrations were controlled by the
105 injection time preset through the electromagnetic valve, and were measured by a NO_x
106 analyzer (Model 42i-TL, Thermo Fisher Scientific, Inc.) and a SO₂ analyzer (Model 43i,
107 Thermo Fisher Scientific Inc.), respectively. In this work, the initial ratio (V/V) of
108 guaiacol concentration to NO_x concentration in the chamber was similar in all
109 experiments (~1.2) (Tables 1 and 2). In addition, sodium chloride (NaCl) and
110 ammonium sulfate ((NH₄)₂SO₄) were used as the inorganic seeds. The seed aerosols in
111 the chamber were generated by the atomization of a 0.02 M aqueous solution. Through
112 atomization, the size distribution of seed particles peaked at 51–58 nm with a number
113 concentration of 10100–11400 cm⁻³ was achieved (Table 2). After gas species and seed
114 particles in the chamber were mixed well, the photooxidation experiment was carried
115 out with the fan turned off. In this work, the OH concentrations in the chamber were
116 (1.3–2.2) × 10⁶ molecules cm⁻³, calculated based on the degradation rate (7.53 × 10⁻¹¹
117 cm³ molecule⁻¹ s⁻¹) of guaiacol with OH radicals (Coeur-Tourneur et al., 2010a). The
118 chemicals and gas samples used in this work were described in Supporting Information.

119 An Aerodyne high-resolution time-of-flight aerosol mass spectrometer (HR-ToF-
120 AMS) was applied to online measure the chemical composition of particles and the non-
121 refractory submicron aerosol mass (DeCarlo et al., 2006). The size distribution and
122 concentration of particles were monitored by a scanning mobility particle sizer (SMPS),



123 which is composed of a differential mobility analyzer (DMA) (Model 3082, TSI Inc.)
124 and a condensation particle counter (CPC) (Model 3776, TSI Inc.). Assuming that
125 particles are spherical and non-porous, the average particle density could be calculated
126 to be 1.4 g cm^{-3} using the equation $\rho = d_{va}/d_m$ (DeCarlo et al., 2004), where d_{va} is the
127 mean vacuum aerodynamic diameter measured by HR-ToF-AMS and d_m is the mean
128 volume-weighted mobility diameter measured by SMPS. The mass concentration of
129 particles measured by HR-ToF-AMS was corrected by SMPS data in this work using
130 the same method as Gordon et al. (2014). In this work, the wall loss rate (k_{dep}) of
131 $(\text{NH}_4)_2\text{SO}_4$ particles could be expressed as $k_{dep} = 4.15 \times 10^{-7} \times D_p^{1.89} + 1.39 \times D_p^{-0.88}$
132 (D_p is the particle diameter (nm)), which was measured according to the literature
133 method (Takekawa et al., 2003) and used to correct the wall loss of SOA. In addition,
134 its wall loss rate was determined at predetermined time intervals, which only had a
135 slight change among different experiments.

136 **3 Results and discussion**

137 **3.1 SOA yields**

138 A series of experiments were conducted at different guaiacol/ NO_x concentrations under
139 atmospheric pressure. The experimental conditions and results are shown in Table 1.
140 SOA yield was calculated to be the ratio of SOA mass concentration (M_0 , $\mu\text{g m}^{-3}$) to the
141 consumed guaiacol concentration ($\Delta[\text{guaiacol}]$, $\mu\text{g m}^{-3}$) at the end of each experiment
142 (Kang et al., 2007). The results showed that SOA yield was dependent on the initial
143 guaiacol concentration. Higher precursor concentration would result in higher amount



144 of condensable products, subsequently enhancing SOA formation (Lauraguais et al.,
145 2012). In addition, it should be noted that SOA mass could directly affect the
146 gas/particle partitioning via acting as the adsorption medium of oxidation products, thus
147 higher SOA mass generally leads to higher SOA yield (Lauraguais et al., 2014b).

148 SOA yield (Y) could be represented by a widely-used semi-empirical model based
149 on the absorptive gas-particle partitioning of semi-volatile products, typically
150 calculated using the following equation (Odum et al., 1996):

$$151 \quad Y = \sum_i M_0 \frac{\alpha_i K_{om,i}}{1 + K_{om,i} M_0} \quad (1)$$

152 where α_i is the mass-based stoichiometric coefficient for the reaction producing the
153 semi-volatile product i , $K_{om,i}$ is the gas-particle partitioning equilibrium constant, and
154 M_0 is the total aerosol mass concentration.

155 The yield curve for guaiacol photooxidation is shown in Fig. 1, obtained by plotting
156 the SOA yield data in Table 1 according to Eq. (1). The yield data were accurately
157 reproduced by a one-product model ($R^2 = 0.97$), while two or more products used in the
158 model did not significantly improve the fitting quality. The obtained values of α_i and
159 $K_{om,i}$ for one-product model were (0.27 ± 0.01) and $(0.033 \pm 0.008) \text{ m}^3 \mu\text{g}^{-1}$, respectively.
160 In previous studies, the one-product model was widely applied to describe SOA yields
161 from the oxidation of aromatic compounds including methoxyphenols (Coeur-Tourneur
162 et al., 2010b; Lauraguais et al., 2012, 2014b). In this work, this simulation suggests that
163 the products in SOA have similar values of α_i and $K_{om,i}$, i.e., the obtained α_i and $K_{om,i}$
164 are the average values. The plot shown in Fig. S2 is the relationship between M_0 versus



165 $\Delta[\text{guaiacol}]$, of which slope (0.28) is slightly higher than α_i value (0.27). This suggests
166 that the formed low-volatile products almost completely partitioned on the particle-
167 phase according to the theoretical partition model (Lauraguais et al., 2012, 2014b).

168 In the previous studies, the significant SOA formation from the OH-initiated
169 reaction of guaiacol has been reported (Lauraguais et al., 2014b; Sun et al., 2010; Yee
170 et al., 2013). In this work, SOA yields for guaiacol photooxidation range from
171 9.46–26.37%, shown in Table 1. This range overlaps SOA yields of 0.6–87% for
172 guaiacol oxidation under high NO_x condition (~ 10 ppm NO), reported by Lauraguais et
173 al. (2014b), using CH_3ONO as the OH source. Under low NO_x conditions (< 5 ppb NO),
174 SOA yields for guaiacol oxidation were in the range of 44–50%, reported by Yee et al.
175 (2013) using H_2O_2 as the OH source and $(\text{NH}_4)_2\text{SO}_4$ as seed particles; they also
176 indicated that high NO_x concentration (> 200 ppb NO) played an opposite role in SOA
177 formation. Compared to the reported results, SOA yields obtained in this work were
178 lower, which might be explained by the different experimental conditions, e.g., OH
179 concentrations and seed particles. For example, Sun et al. (2010) have reported that
180 SOA mass formed from the aqueous-phase photochemical reaction of guaiacol in the
181 presence of H_2O_2 is about one-fold higher than that in the absence of H_2O_2 .

182 In addition, the average N/C ratio of SOA for guaiacol photooxidation in the
183 presence of NO_x is 0.037, calculated according to the element analysis by HR-ToF-
184 AMS. This indicates that NO_x incorporates in guaiacol photooxidation. This
185 phenomenon is well supported by the previous results, which reported that the nitro-



186 substituted products are the main products of the OH-initiated reaction of guaiacol in
187 the presence of NO_x (Ahmad et al., 2017; Lauraguais et al., 2014b). The relative low
188 volatility of these products could reasonably contribute to SOA formation (Duport et
189 al., 2016; Liu et al., 2016a). The average NO⁺/NO₂⁺ ratio of SOA from guaiacol
190 photooxidation is 4.08, which is within the range of 3.82–5.84 for organic nitrates of
191 SOA from the photooxidation of aromatics (Sato et al., 2010). In this work, the
192 measured NO⁺/NO₂⁺ ratios for inorganic nitrates are in the range of 2.06 to 2.54,
193 determined by HR-ToF-AMS using ammonium nitrate as calibration sample. The
194 relative abundance of organic nitrates could be estimated from the average N/C ratio.
195 Assuming that the oxidation products in the SOA retain 7 carbon atoms, the yield of
196 organic nitrates is 25.9%, which is the upper limit due to the possible C–C bond
197 scission during photooxidation process.

198 **3.2 Effect of SO₂ on SOA formation**

199 In China, atmospheric SO₂ concentration is always in the range of several to dozens of
200 ppb, while in the severely polluted atmosphere it could be up to close 200 ppb (Han et
201 al., 2015; Li et al., 2017). In addition, a recent field measurement study has reported
202 that the decrease of biogenic SOA mass concentration in the atmosphere has a positive
203 correlation with SO₂ emission controls (Marais et al., 2017). Therefore, the effect of
204 SO₂ at atmospheric levels on SOA formation from guaiacol photooxidation under
205 atmospheric NO_x conditions was investigated. The experimental conditions and results
206 are shown in Table 2. The formation of SOA, sulfate, and nitrate as a function of SO₂



207 concentration for guaiacol photooxidation is shown in Fig. S3. As illustrated in Fig. 2,
208 M_0 for the blank experiment (Expt. 1 in Table 2) increased from 63.62 to 71.88 and
209 $78.59 \mu\text{g m}^{-3}$, enhanced by 12.98% and 23.53%, respectively, when SO_2 concentration
210 raised from 0 to 33 and 56 ppb. The corresponding SOA yield increased by 14.05% and
211 23.66%, respectively. The similar results were reported by previous studies (Kleindienst
212 et al., 2006; Lin et al., 2013; Liu et al., 2016b), which observed the significant
213 enhancements of SOA yields for VOCs oxidation and the photochemical aging of
214 gasoline vehicle exhaust in the presence of SO_2 .

215 The average carbon oxidation state ($\text{OS}_C = 2\text{O}/\text{C} - \text{H}/\text{C}$) of OA is widely used to
216 represent the oxidation degree of atmospheric OA, because it takes into account the
217 saturation level of carbon atoms in the OA (Kroll et al., 2011). As shown in Table 2,
218 increasing SO_2 concentration (0–56 ppb) leads to the increase of OS_C (0.11–0.18). In
219 order to further identify the effect of SO_2 on the chemical properties of SOA, positive
220 matrix factorization (PMF) analysis for the AMS data obtained at different SO_2
221 concentrations was carried out. Two factors were obtained from the PMF analysis, and
222 their mass spectra are shown in Fig. 3. The organic mass fraction of m/z 44 (CO_2^+),
223 named f_{44} , was 0.122 for Factor 2, which is higher than that (0.094) for Factor 1.
224 Therefore, Factor 2 was tentatively assigned to the more-oxidized SOA, while Factor 1
225 was the less-oxidized SOA (Ulbrich et al., 2009). During the photooxidation process,
226 these two factors had different variations as a function of reaction time. As shown in
227 Fig. S4, Factor 1 decreased along with the reaction, while Factor 2 had an opposite



228 trend. Compared to Expts. 1 and 2 in Table 2, the higher fraction of Factor 2 mass
229 obtained at 56 ppb SO₂ (Expt. 3 in Table 2) suggests that the formed SOA mainly
230 consists of more-oxidized products with relatively low volatility, which is well
231 supported by the obtained OS_C of SOA.

232 Previous studies mostly reported that the enhancement of SOA yield in the presence
233 of SO₂ was ascribed to the functionalization and oligomerization reactions (Cao and
234 Jang, 2007; Jaoui et al., 2008 ; Liu et al., 2016b; Xu et al., 2016). If the oligomerization
235 reaction plays a predominant role in the presence of SO₂ which will lead to particle
236 phase H₂SO₄, the oxidation state of SOA will decrease. Nevertheless, we observed that
237 SO₂ not only enhanced SOA yields, but also resulted in higher OS_C (Table 2 and Fig.
238 4). This suggests that the functionalization reaction should be predominant with SO₂,
239 which leads to higher OS_C of products with low molecular weight (MW) (Ye et al.,
240 2018), consequently resulting in an overall increase in OS_C and SOA yields. More
241 recently, Ye et al. (2018) also found the similar results in the ozonolysis of limonene.
242 Fig. S5 shows the differences among the normalized mass spectra of SOA formed at
243 different SO₂ concentrations. As shown in Fig. S5a, the signal fractions from the low-
244 MW species are enhanced significantly in the presence of SO₂, and are much higher
245 than those from the high-MW species (m/z >300). The similar results are also observed
246 in Fig. S5b when increasing SO₂ concentration. In other words, SO₂ played a more
247 important role in the formation of organosulfate and the formation or uptake of low-
248 WM species, compared to the formation of high-MW species (i.e., oligomers). In this



249 work, organosulfate concentration increased with the increase of SO₂ concentration,
250 and was in the range of 2.1–4.3 ng m⁻³, calculated using the method described by Huang
251 et al. (2015). This concentration range is close to those derived from the atmospheric
252 oxidation of polycyclic aromatic hydrocarbons and alkane (Riva et al., 2015; Meade et
253 al., 2016). Fig. S6 is the examples of the ions (i.e., CSO⁺, CH₃SO₂⁺, and CH₃SO₃⁺)
254 in the calibration of methyl sulfate obtained at 56 ppb SO₂. On the other hand, sulfuric
255 acid formed from SO₂ may be favorable of the uptake of water-soluble low-MW species
256 (e.g., small carboxylic acids and aldehydes), which also results in the increase of OS_C.
257 In addition, Krapf et al. (2016) have indicated that peroxides in SOA are unstable and
258 liable to decompose into volatile compounds, consequently leading to decrease SOA
259 yield and OS_C. But, Ye et al. (2018) recently found that the reactions of SO₂ with organic
260 peroxides were the dominant sink of SO₂, initiated by the heterogeneous uptake of SO₂
261 under humidity condition. These reactions would result in the formation of
262 organosulfates, consequently increasing SOA yields and OS_C.

263 In addition, it has been reported that the formed sulfate by SO₂ oxidation not only
264 serves as the substrate for the condensation of low-volatility vapors (Jaoui et al., 2008),
265 but also increases the surface areas of particles (Xu et al., 2016). These roles of sulfate
266 are also favorable for increasing SOA yields. In the presence of SO₂, however, we did
267 not observe the particle mode attributed to H₂SO₄ formed from SO₂ oxidation.
268 Therefore, we calculated the surface area concentration of aerosol particles at the end
269 time. As shown in Table 2, the final surface area of aerosol particles formed via guaiacol



270 photooxidation increased from 1.25×10^3 to 1.68×10^3 and $2.04 \times 10^3 \mu\text{m}^2 \text{cm}^{-3}$ when
271 SO_2 concentration increased from 0 to 33 and 56 ppb. The increased surface area could
272 be in favor of outcompeting the wall loss for low-volatility vapors produced from
273 guaiacol photooxidation, i.e., more low-volatility vapors will be diverted from wall loss
274 to the particles, consequently increasing SOA yields (Kroll et al., 2007). But, the surface
275 area of aerosol particles is still much lower than that ($1.97 \times 10^6 \mu\text{m}^2 \text{cm}^{-3}$) of smog
276 chamber used in this work. Therefore, the enhancement of SOA yields by the increased
277 surface area from H_2SO_4 by SO_2 oxidation might be limited.

278 3.3 Effect of inorganic seed particles on SOA formation

279 Seed particle is one of the critical factors influencing SOA formation (Ge et al., 2017a),
280 thus the effects of inorganic seeds (NaCl and $(\text{NH}_4)_2\text{SO}_4$) on SOA formation from
281 guaiacol photooxidation were investigated. As shown in Fig. 5, the presence of
282 inorganic seed particles could accelerate SOA growth rate at the initial stage of
283 photooxidation, followed by the decrease of growth rate along with the reaction,
284 because the presence of inorganic seeds could promote the condensation of SOA-
285 forming organic products and consequently increase SOA formation (Yee et al., 2013).
286 The results showed that M_0 for the blank experiment (Expt. 1 in Table 2) increased from
287 63.62 to 79.44 and 84.91 $\mu\text{g m}^{-3}$ (Table 2), enhanced by 24.87% and 33.46%,
288 respectively, with $(\text{NH}_4)_2\text{SO}_4$ and NaCl seed particles. The corresponding SOA yield
289 increased by 23.06% and 29.57%, respectively. In previous work, the similar results
290 about the enhancements of SOA formation by NaCl and $(\text{NH}_4)_2\text{SO}_4$ seed particles were



291 reported in the oxidation of VOCs (Ge et al., 2017a, 2017b; Huang et al., 2013, 2017).

292 As shown in Table 2 and Fig. 5, the SOA mass concentration in the presence of

293 NaCl seed particles is higher than that in the presence of $(\text{NH}_4)_2\text{SO}_4$ seed particles. In

294 addition, OS_C of SOA in the presence of NaCl seed particles is 0.29, slightly higher

295 than that (0.20) in the presence of $(\text{NH}_4)_2\text{SO}_4$ seed particles. Recently, it has been also

296 reported that the presence of $(\text{NH}_4)_2\text{SO}_4$ and NaNO_3 seed particles could enhance

297 significantly the oxidation state of SOA, compared to without seed particles (Huang et

298 al., 2016). In this work, the experimental conditions for seed experiments are almost

299 the same (Table 2), including reactant concentration, temperature, RH, and the number

300 and diameter of seed particles. Therefore, the differences in the yield and oxidation state

301 of SOA were reasonably resulted from the different chemical compositions of SOA with

302 different inorganic seeds. Fig. 6 shows the mass spectra of SOA in the presence of NaCl

303 and $(\text{NH}_4)_2\text{SO}_4$ seed particles obtained by HR-ToF-AMS, as well as their difference

304 mass spectrum. As shown in Fig. 6, f_{44} and the organic mass fraction of m/z 28 (CO^+)

305 for SOA in the presence of NaCl seed particles are both higher than those in the presence

306 of $(\text{NH}_4)_2\text{SO}_4$ seed particles, while the mass fractions of CH_3 and CHO fragments are

307 both lower. The m/z 44 ion (CO_2^+) is mainly contributed from acids or acid-derived

308 species, such as esters (Ng et al., 2011). The higher f_{44} of SOA with NaCl than

309 $(\text{NH}_4)_2\text{SO}_4$ seed particles suggests that the distribution of highly oxidized small

310 carboxylic acids onto seed particles plays an important role in SOA formation,

311 consequently resulting in higher oxidation state of SOA (Ng et al., 2011; Huang et al.,



312 2016). Compared to $(\text{NH}_4)_2\text{SO}_4$, the hygroscopicity of NaCl is stronger (Ge et al., 2017a;
313 Gysel et al., 2002). The molar ratio of H_2O to NaCl is about 0.1 at 40% RH, and water
314 is mainly adsorbed on NaCl particles (Weis and Ewing, 1999). Thus, the greater water
315 content on the particle surface could facilitate the uptake of highly oxidized small
316 carboxylic acids onto NaCl particles, which might be potentially explain the higher
317 SOA oxidation state observed in the presence of NaCl seed particles (Huang et al.,
318 2016). The adsorbed acid products would also generate H^+ ions, which could catalyze
319 heterogeneous reactions to produce more-oxidized products or oligomers with
320 relatively low volatility (Fig. S7), consequently resulting in the enhancement of SOA
321 formation (Huang et al., 2013, 2017; Cao and Jang, 2007; Jaoui et al., 2008; Liu et al.,
322 2016b; Xu et al., 2016).

323 In addition, the possible formation of Cl atoms from the photolysis of nitryl
324 chloride ($\text{ClNO}_2 \xrightarrow{h\nu} \text{Cl} + \text{NO}_2$, $k_1 = \sim 10^{-4} \text{ s}^{-1}$) (Mielke et al., 2011) and the reaction
325 of OH radical with Cl^- ($\text{Cl}^- + \text{OH} \rightarrow \text{Cl} + \text{OH}^-$, $k_2 = \sim 10^9 \text{ M}^{-1} \text{ s}^{-1}$) (Fang et al., 2014)
326 would also initiate a series of reactions to oxidize SOA composition, which might be
327 another reason for higher OS_c observed with NaCl seed particles. According to the rate
328 constant ($10^9 \text{ M}^{-1} \text{ s}^{-1}$) (Fang et al., 2014), the uptake coefficient (3.4×10^{-3}) of OH
329 radicals on NaCl particles (Park et al., 2008), and the concentrations of OH radicals and
330 Cl^- , the concentration of Cl atoms from the reaction of OH radical with Cl^- was
331 estimated to be less than $38 \text{ molecules cm}^{-3}$, which was much higher than that from the
332 photolysis of ClNO_2 due to the slow photolysis rate constant of $\sim 10^{-4} \text{ s}^{-1}$ (Mielke et



333 al., 2011). Compared to OH concentration in the chamber, the oxidation of SOA
334 composition by Cl atoms should be insignificant.

335 **3.4 Synergetic effect of SO₂ and inorganic seed particles on SOA formation**

336 According to the former results obtained in this work, it is clearly known that SO₂ and
337 inorganic seed particles both have a positive role in enhancing SOA formation.
338 Therefore, their possible synergetic effects on SOA formation were investigated. In
339 view of the experiments performed under the comparable conditions (Table 2), the
340 results should be reasonably reliable. As shown in Fig. 7, the addition of SO₂ into the
341 chamber in the presence of inorganic seed particles significantly promotes SOA
342 formation from guaiacol photooxidation. When SO₂ concentration raised from 0 to 30
343 and 54 ppb in the presence of NaCl seed particles, M₀ was enhanced by 42.86% and
344 55.39%, respectively, and the corresponding SOA yield increased by 41.43% and
345 53.47%, compared to the blank experiment (Expt. 1 in Table 2). For (NH₄)₂SO₄ seed
346 particles, M₀ was enhanced by 32.58% for 33 ppb SO₂ and 41.34% for 54 ppb SO₂,
347 respectively, and the corresponding SOA yield increased by 29.78% and 39.24%.
348 Therefore, inorganic seed particles and SO₂ have a synergistic effect on SOA formation.

349 As shown in Table 2 and Fig. 4, it should be noted that OS_C of SOA increases in
350 the presence of SO₂. Fig. S8 shows the mass spectra of SOA with NaCl and (NH₄)₂SO₄
351 as seed particles at different SO₂ concentrations obtained by HR-ToF-AMS. As
352 illustrated in Fig. S8, SO₂ addition is in favor of increasing the value of *f*₄₄, suggesting
353 that more products with higher OS_C are produced by the functionalization reaction (Ye



354 et al., 2018). Meanwhile, Table 2 shows that the final surface area of aerosol particles
355 increased in the presence of SO₂, which played a positive role in diverting more low-
356 volatility vapors from wall loss to the particles, consequently enhancing SOA yields
357 (Kroll et al., 2007). But, this impact should be insignificant due to the much lower
358 surface area of aerosol particles compared to that ($1.97 \times 10^6 \mu\text{m}^2 \text{cm}^{-3}$) of smog
359 chamber in this work. In addition, the presence of inorganic seeds could promote the
360 condensation of SOA-forming organic products and the heterogeneous uptake of SO₂
361 (Yee et al., 2013), providing favorable conditions for the following oxidation reactions.
362 Meanwhile, the higher hygroscopicity of NaCl than (NH₄)₂SO₄ might be helpful to
363 dissolve more acid substances on NaCl particle surface (e.g., H₂SO₄ and organic acid),
364 especially in the presence of SO₂, which might be helpful to catalyze heterogeneous
365 reactions (Cao and Jang, 2007; Huang et al., 2013, 2017; Jaoui et al., 2008; Liu et al.,
366 2016b; Xu et al., 2016). Figs. S9 and S10 show the differences among the normalized
367 mass spectra of SOA formed at different SO₂ concentrations with various seed particles,
368 which both shows that the signal fractions from the low-MW species are increased
369 significantly in the presence of SO₂, and are much higher than those from the high-MW
370 species ($m/z > 300$). Compared to Expts. 2 and 3 in Table 2 with no seed particles,
371 organosulfate concentrations formed with seed particles were similar and in the range
372 of 2.2–4.6 ng m⁻³, which might be caused by the similar SO₂ concentrations applied for
373 experiments. With NaCl and (NH₄)₂SO₄ as seed particles, SOA yields and OS_C both
374 also increased with the increase of SO₂, suggesting that the functionalization reaction



375 should be more dominant than oligomerization reaction during photooxidation process.

376 **4 Conclusions and atmospheric implications**

377 In this work, SOA formation from guaiacol photooxidation in the presence of NO_x was
378 investigated in a 30 m^3 smog chamber. SOA yields for guaiacol photooxidation were in
379 the range of 9.46–26.37% at the initial guaiacol concentrations ranging from
380 $138.83\text{--}2197.36 \mu\text{g m}^{-3}$, and could be expressed well by a one-product model. The
381 presence of SO_2 could increase SOA yield and OS_C , indicating that the functionalization
382 reaction should be more dominant than oligomerization reaction. Meanwhile, the
383 similar effect of SO_2 was also observed with NaCl and $(\text{NH}_4)_2\text{SO}_4$ seed particles. But,
384 SOA yield and OS_C in the presence of NaCl seed particles were both slightly higher
385 than those in the presence of $(\text{NH}_4)_2\text{SO}_4$ seed particles. In addition, the results indicated
386 the synergetic contribution of SO_2 and inorganic seed particles to SOA formation. The
387 average N/C ratio (0.037) of SOA suggested that NO_x participated in the process of
388 guaiacol photooxidation, resulting in the formation of organic nitrates.

389 The significant SOA formation from guaiacol photooxidation at the atmospheric
390 levels of SO_2 and NO_x in this work suggests that it should pay more attention on the
391 SOA formation from biomass burning and its subsequent effects on haze evolution,
392 especially in China with nationwide biomass burning, because recent studies have
393 indicated that SOA formed from biomass burning plays an important role in haze
394 pollution in China (Ding et al., 2017; Li et al., 2017). In addition, the results imply that
395 the oxidation of SO_2 and VOCs should be tightly combined, and SO_2 has a direct impact



396 on the chemistry of SOA formation. Although guaiacol concentrations in the chamber
397 study are higher than those in the ambient atmosphere, the results obtained in this work
398 could provide new information for SOA formation from the photooxidation of
399 methoxyphenols, and might be useful for SOA modeling, especially for air quality
400 simulation modeling of the specific regions experiencing serious pollution caused by
401 fine particulate matter. In addition, the results would help to further understand the
402 photochemical aging process of smoke plumes from biomass burning in the atmosphere.

403 **Data availability**

404 The experimental data are available upon request to the corresponding authors.

405 **Competing interests**

406 The authors declare that they have no conflict of interest.

407 **Acknowledgements**

408 This work was financially supported by the National Key R&D Program of China
409 (2016YFC0202700), the National Natural Science Foundation of China (21607088),
410 China Postdoctoral Science Foundation funded project (2017M620071), and the
411 Applied Basic Research Project of Science and Technology Department of Sichuan
412 Province (2018JY0303). Liu Y. would like to thank Beijing University of Chemical
413 Technology for financial supporting. Authors would also acknowledge the
414 experimental help provided by Dr. Xiaolei Bao from Hebei Provincial Academy of
415 Environmental Sciences, Shijiazhuang, China.

416 **References**

- 417 Ahmad, W., Coeur, C., Tomas, A., Fagniez, T., Brubach, J.-B., and Cuisset, A.: Infrared
418 spectroscopy of secondary organic aerosol precursors and investigation of the
419 hygroscopicity of SOA formed from the OH reaction with guaiacol and syringol,
420 *Appl. Opt.*, 56, E116-E122, doi: 10.1364/ao.56.00e116, 2017.
- 421 Bari, M. A., and Kindzierski, W. B.: Fine particulate matter (PM_{2.5}) in Edmonton,
422 Canada: Source apportionment and potential risk for human health, *Environ.*
423 *Pollut.*, 218, 219-229, doi: 10.1016/j.envpol.2016.06.014, 2016.
- 424 Cao, G., and Jang, M.: Effects of particle acidity and UV light on secondary organic
425 aerosol formation from oxidation of aromatics in the absence of NO_x, *Atmos.*
426 *Environ.*, 41, 7603-7613, doi: 10.1016/j.atmosenv.2007.05.034, 2007.
- 427 Chen, Y., and Bond, T. C.: Light absorption by organic carbon from wood combustion,
428 *Atmos. Chem. Phys.*, 10, 1773-1787, doi: 10.5194/acp-10-1773-2010, 2010.
- 429 Chou, C. C. K., Tsai, C. Y., Chang, C. C., Lin, P. H., Liu, S. C., and Zhu, T.:
430 Photochemical production of ozone in Beijing during the 2008 Olympic Games,
431 *Atmos. Chem. Phys.*, 11, 9825-9837, doi: 10.5194/acp-11-9825-2011, 2011.
- 432 Chu, B., Zhang, X., Liu, Y., He, H., Sun, Y., Jiang, J., Li, J., and Hao, J.: Synergetic
433 formation of secondary inorganic and organic aerosol: Effect of SO₂ and NH₃ on
434 particle formation and growth, *Atmos. Chem. Phys.*, 16, 14219-14230, doi:
435 10.5194/acp-16-14219-2016, 2016.
- 436 Chu, B., Liggio, J., Liu, Y., He, H., Takekawa, H., Li, S.-M., and Hao, J.: Influence of
437 metal-mediated aerosol-phase oxidation on secondary organic aerosol formation
438 from the ozonolysis and OH-oxidation of α -pinene, *Sci. Rep.*, 7, 40311, doi:
439 10.1038/srep40311, 2017.
- 440 Coeur-Tourneur, C., Cassez, A., and Wenger, J. C.: Rate coefficients for the gas-phase
441 reaction of hydroxyl radicals with 2-methoxyphenol (guaiacol) and related
442 compounds, *J. Phys. Chem. A*, 114, 11645-11650, doi: 10.1021/jp1071023, 2010a.
- 443 Coeur-Tourneur, C., Foulon, V., and Lareal, M.: Determination of aerosol yields from
444 3-methylcatechol and 4-methylcatechol ozonolysis in a simulation chamber,
445 *Atmos. Environ.*, 44, 852-857, doi: 10.1016/j.atmosenv.2009.11.027, 2010b.
- 446 DeCarlo, P. F., Slowik, J. G., Worsnop, D. R., Davidovits, P., and Jimenez, J. L.: Particle
447 morphology and density characterization by combined mobility and aerodynamic
448 diameter measurements. Part 1: Theory, *Aerosol Sci. Technol.*, 38, 1185-1205, doi:
449 10.1080/027868290903907, 2004.
- 450 DeCarlo, P. F., Kimmel, J. R., Trimborn, A., Northway, M. J., Jayne, J. T., Aiken, A. C.,
451 Gonin, M., Fuhrer, K., Horvath, T., Docherty, K. S., Worsnop, D. R., and Jimenez,
452 J. L.: Field-deployable, high-resolution, time-of-flight aerosol mass spectrometer,
453 *Anal. Chem.*, 78, 8281-8289, doi: 10.1021/ac061249n, 2006.
- 454 Ding, X., Zhang, Y.-Q., He, Q.-F., Yu, Q.-Q., Wang, J.-Q., Shen, R.-Q., Song, W., Wang,
455 Y.-S., and Wang, X.-M.: Significant increase of aromatics-derived secondary
456 organic aerosol during fall to winter in China, *Environ. Sci. Technol.*, 51, 7432-



- 457 7441, doi: 10.1021/acs.est.6b06408, 2017.
- 458 Duporté G., Parshintsev, J., Barreira, L. M. F., Hartonen, K., Kulmala, M., and
459 Riekkola, M.-L.: Nitrogen-containing low volatile compounds from
460 pinonaldehyde-dimethylamine reaction in the atmosphere: A laboratory and field
461 study, *Environ. Sci. Technol.*, 50, 4693-4700, doi: 10.1021/acs.est.6b00270, 2016.
- 462 El Zein, A., Coeur, C., Obeid, E., Lauraguais, A., and Fagniez, T.: Reaction kinetics of
463 catechol (1,2-benzenediol) and guaiacol (2-methoxyphenol) with ozone, *J. Phys.
464 Chem. A*, 119, 6759-6765, doi: 10.1021/acs.jpca.5b00174, 2015.
- 465 Fang, J., Fu, Y., and Shang, C.: The roles of reactive species in micropollutant
466 degradation in the UV/free chlorine system, *Environ. Sci. Technol.*, 48, 1859-1868,
467 doi: 10.1021/es4036094, 2014.
- 468 Ge, S., Xu, Y., and Jia, L.: Effects of inorganic seeds on secondary organic aerosol
469 formation from photochemical oxidation of acetone in a chamber, *Atmos. Environ.*,
470 170, 205-215, doi: 10.1016/j.atmosenv.2017.09.036, 2017a.
- 471 Ge, S., Xu, Y., and Jia, L.: Secondary organic aerosol formation from propylene
472 irradiations in a chamber study, *Atmos. Environ.*, 157, 146-155, doi:
473 10.1016/j.atmosenv.2017.03.019, 2017b.
- 474 Gordon, T. D., Presto, A. A., Nguyen, N. T., Robertson, W. H., Na, K., Sahay, K. N.,
475 Zhang, M., Maddox, C., Rieger, P., Chattopadhyay, S., Maldonado, H., Maricq, M.
476 M., and Robinson, A. L.: Secondary organic aerosol production from diesel
477 vehicle exhaust: impact of aftertreatment, fuel chemistry and driving cycle, *Atmos.
478 Chem. Phys.*, 14, 4643-4659, doi: 10.5194/acp-14-4643-2014, 2014.
- 479 Gysel, M., Weingartner, E., and Baltensperger, U.: Hygroscopicity of aerosol particles
480 at low temperatures. 2. Theoretical and experimental hygroscopic properties of
481 laboratory generated aerosols, *Environ. Sci. Technol.*, 36, 63-68, doi:
482 10.1021/es010055g, 2002.
- 483 Han, T., Liu, X., Zhang, Y., Qu, Y., Zeng, L., Hu, M., and Zhu, T.: Role of secondary
484 aerosols in haze formation in summer in the Megacity Beijing, *J. Environ. Sci.*, 31,
485 51-60, doi: 10.1016/j.jes.2014.08.026, 2015.
- 486 Hawthorne, S. B., Krieger, M. S., Miller, D. J., and Mathiason, M. B.: Collection and
487 quantitation of methoxylated phenol tracers for atmospheric pollution from
488 residential wood stoves, *Environ. Sci. Technol.*, 23, 470-475, doi:
489 10.1021/es00181a013, 1989.
- 490 Hawthorne, S. B., Miller, D. J., Langenfeld, J. J., and Krieger, M. S.: PM10 high-
491 volume collection and quantitation of semivolatile and nonvolatile phenols,
492 methoxylated phenols, alkanes, and polycyclic aromatic hydrocarbons from winter
493 urban air and their relationship to wood smoke emissions, *Environ. Sci. Technol.*,
494 26, 2251-2262, doi: 10.1021/es00035a026, 1992.
- 495 Huang, D. D., Li, Y. J., Lee, B. P., and Chan, C. K.: Analysis of organic sulfur
496 compounds in atmospheric aerosols at the HKUST supersite in Hong Kong using
497 HR-ToF-AMS, *Environ. Sci. Technol.*, 49, 3672-3679, doi: 10.1021/es5056269,
498 2015.



- 499 Huang, D. D., Zhang, X., Dalleska, N. F., Lignell, H., Coggon, M. M., Chan, C.-M.,
500 Flagan, R. C., Seinfeld, J. H., and Chan, C. K.: A note on the effects of inorganic
501 seed aerosol on the oxidation state of secondary organic aerosol-alpha-Pinene
502 ozonolysis, *J. Geophys. Res.-Atmos.*, 121, 12476-12483, doi:
503 10.1002/2016jd025999, 2016.
- 504 Huang, M., Hao, L., Gu, X., Hu, C., Zhao, W., Wang, Z., Fang, L., and Zhang, W.:
505 Effects of inorganic seed aerosols on the growth and chemical composition of
506 secondary organic aerosol formed from OH-initiated oxidation of toluene, *J.*
507 *Atmos. Chem.*, 70, 151-164, doi: 10.1007/s10874-013-9262-9, 2013.
- 508 Huang, M., Hao, L., Cai, S., Gu, X., Zhang, W., Hu, C., Wang, Z., Fang, L., and Zhang,
509 W.: Effects of inorganic seed aerosols on the particulate products of aged 1,3,5-
510 trimethylbenzene secondary organic aerosol, *Atmos. Environ.*, 152, 490-502, doi:
511 10.1016/j.atmosenv.2017.01.010, 2017.
- 512 Jaoui, M., Edney, E. O., Kleindienst, T. E., Lewandowski, M., Offenber, J. H., Surratt,
513 J. D., and Seinfeld, J. H.: Formation of secondary organic aerosol from irradiated
514 alpha-pinene/toluene/NO_x mixtures and the effect of isoprene and sulfur dioxide,
515 *J. Geophys. Res.-Atmos.*, 113, doi: 10.1029/2007jd009426, 2008.
- 516 Kang, E., Root, M. J., Toohey, D. W., and Brune, W. H.: Introducing the concept of
517 Potential Aerosol Mass (PAM), *Atmos. Chem. Phys.*, 7, 5727-5744, doi:
518 10.5194/acp-7-5727-2007, 2007.
- 519 Kleindienst, T. E., Edney, E. O., Lewandowski, M., Offenber, J. H., and Jaoui, M.:
520 Secondary organic carbon and aerosol yields from the irradiations of isoprene and
521 alpha-pinene in the presence of NO_x and SO₂, *Environ. Sci. Technol.*, 40, 3807-
522 3812, doi: 10.1021/es052446r, 2006.
- 523 Krapf, M., El Haddad, I., Bruns, E. A., Molteni, U., Daellenbach, K. R., Prevot, A. S.
524 H., Baltensperger, U., and Dommen, J.: Labile peroxides in secondary organic
525 aerosol, *Chem*, 1, 603-616, doi: 10.1016/j.chempr.2016.09.007, 2016.
- 526 Kroll, J. H., Chan, A. W. H., Ng, N. L., Flagan, R. C., and Seinfeld, J. H.: Reactions of
527 semivolatile organics and their effects on secondary organic aerosol formation,
528 *Environ. Sci. Technol.*, 41, 3545-3550, doi: 10.1021/es062059x, 2007.
- 529 Kroll, J. H., Donahue, N. M., Jimenez, J. L., Kessler, S. H., Canagaratna, M. R., Wilson,
530 K. R., Altieri, K. E., Mazzoleni, L. R., Wozniak, A. S., Bluhm, H., Mysak, E. R.,
531 Smith, J. D., Kolb, C. E., and Worsnop, D. R.: Carbon oxidation state as a metric
532 for describing the chemistry of atmospheric organic aerosol, *Nature Chem.*, 3, 133-
533 139, doi: 10.1038/nchem.948, 2011.
- 534 Lauraguais, A., Coeur-Tourneur, C., Cassez, A., and Seydi, A.: Rate constant and
535 secondary organic aerosol yields for the gas-phase reaction of hydroxyl radicals
536 with syringol (2,6-dimethoxyphenol), *Atmos. Environ.*, 55, 43-48, doi:
537 10.1016/j.atmosenv.2012.02.027, 2012.
- 538 Lauraguais, A., Bejan, I., Barnes, I., Wiesen, P., Coeur-Tourneur, C., and Cassez, A.:
539 Rate coefficients for the gas-phase reaction of chlorine atoms with a series of
540 methoxylated aromatic compounds, *J. Phys. Chem. A*, 118, 1777-1784, doi:



- 541 10.1021/jp4114877, 2014a.
- 542 Lauraguais, A., Coeur-Tourneur, C., Cassez, A., Deboudt, K., Fourmentin, M., and
543 Choel, M.: Atmospheric reactivity of hydroxyl radicals with guaiacol (2-
544 methoxyphenol), a biomass burning emitted compound: Secondary organic
545 aerosol formation and gas-phase oxidation products, *Atmos. Environ.*, 86, 155-
546 163, doi: 10.1016/j.atmosenv.2013.11.074, 2014b.
- 547 Lauraguais, A., El Zein, A., Coeur, C., Obeid, E., Cassez, A., Rayez, M.-T., and Rayez,
548 J.-C.: Kinetic study of the gas-phase reactions of nitrate radicals with
549 methoxyphenol compounds: Experimental and theoretical approaches, *J. Phys.*
550 *Chem. A*, 120, 2691-2699, doi: 10.1021/acs.jpca.6b02729, 2016.
- 551 Lelieveld, J., Crutzen, P. J., Ramanathan, V., Andreae, M. O., Brenninkmeijer, C. A. M.,
552 Campos, T., Cass, G. R., Dickerson, R. R., Fischer, H., de Gouw, J. A., Hansel, A.,
553 Jefferson, A., Kley, D., de Laat, A. T. J., Lal, S., Lawrence, M. G., Lobert, J. M.,
554 Mayol-Bracero, O. L., Mitra, A. P., Novakov, T., Oltmans, S. J., Prather, K. A.,
555 Reiner, T., Rodhe, H., Scheeren, H. A., Sikka, D., and Williams, J.: The Indian
556 Ocean Experiment: Widespread air pollution from South and Southeast Asia,
557 *Science*, 291, 1031-1036, doi: 10.1126/science.1057103, 2001.
- 558 Li, H., Zhang, Q., Zhang, Q., Chen, C., Wang, L., Wei, Z., Zhou, S., Parworth, C.,
559 Zheng, B., Canonaco, F., Prevot, A. S. H., Chen, P., Zhang, H., Wallington, T. J.,
560 and He, K.: Wintertime aerosol chemistry and haze evolution in an extremely
561 polluted city of the North China Plain: Significant contribution from coal and
562 biomass combustion, *Atmos. Chem. Phys.*, 17, 4751-4768, doi: 10.5194/acp-17-
563 4751-2017, 2017.
- 564 Lin, Y. H., Knipping, E. M., Edgerton, E. S., Shaw, S. L., and Surratt, J. D.:
565 Investigating the influences of SO₂ and NH₃ levels on isoprene-derived secondary
566 organic aerosol formation using conditional sampling approaches, *Atmos. Chem.*
567 *Phys.*, 13, 8457-8470, doi: 10.5194/acp-13-8457-2013, 2013.
- 568 Liu, J., Lin, P., Laskin, A., Laskin, J., Kathmann, S. M., Wise, M., Caylor, R., Imholt,
569 F., Selimovic, V., and Shilling, J. E.: Optical properties and aging of light-
570 absorbing secondary organic aerosol, *Atmos. Chem. Phys.*, 16, 12815-12827, doi:
571 10.5194/acp-16-12815-2016, 2016a.
- 572 Liu, T., Wang, X., Hu, Q., Deng, W., Zhang, Y., Ding, X., Fu, X., Bernard, F., Zhang,
573 Z., Lu, S., He, Q., Bi, X., Chen, J., Sun, Y., Yu, J., Peng, P., Sheng, G., and Fu, J.:
574 Formation of secondary aerosols from gasoline vehicle exhaust when mixing with
575 SO₂, *Atmos. Chem. Phys.*, 16, 675-689, doi: 10.5194/acp-16-675-2016, 2016b.
- 576 Marais, E. A., Jacob, D. J., Turner, J. R., and Mickley, L. J.: Evidence of 1991-2013
577 decrease of biogenic secondary organic aerosol in response to SO₂ emission
578 controls, *Environ. Res. Lett.*, 12, doi: 10.1088/1748-9326/aa69c8, 2017.
- 579 Meade, L. E., Riva, M., Blomberg, M. Z., Brock, A. K., Qualters, E. M., Siejack, R. A.,
580 Ramakrishnan, K., Surratt, J. D., and Kautzman, K. E.: Seasonal variations of fine
581 particulate organosulfates derived from biogenic and anthropogenic hydrocarbons
582 in the mid-Atlantic United States, *Atmos. Environ.*, 145, 405-414, doi:



- 583 10.1016/j.atmosenv.2016.09.028, 2016.
- 584 Mielke, L. H., Furgeson, A., and Osthoff, H. D.: Observation of ClNO₂ in a mid-
585 continental urban environment, *Environ. Sci. Technol.*, 45, 8889-8896, doi:
586 10.1021/es201955u, 2011.
- 587 Naeher, L. P., Brauer, M., Lipsett, M., Zelikoff, J. T., Simpson, C. D., Koenig, J. Q., and
588 Smith, K. R.: Woodsmoke health effects: A review, *Inhal. Toxicol.*, 19, 67-106,
589 doi: 10.1080/08958370600985875, 2007.
- 590 Ng, N. L., Chhabra, P. S., Chan, A. W. H., Surratt, J. D., Kroll, J. H., Kwan, A. J.,
591 McCabe, D. C., Wennberg, P. O., Sorooshian, A., Murphy, S. M., Dalleska, N. F.,
592 Flagan, R. C., and Seinfeld, J. H.: Effect of NO_x level on secondary organic aerosol
593 (SOA) formation from the photooxidation of terpenes, *Atmos. Chem. Phys.*, 7,
594 5159-5174, doi: 10.5194/acp-7-5159-2007, 2007.
- 595 Ng, N. L., Canagaratna, M. R., Jimenez, J. L., Chhabra, P. S., Seinfeld, J. H., and
596 Worsnop, D. R.: Changes in organic aerosol composition with aging inferred from
597 aerosol mass spectra, *Atmos. Chem. Phys.*, 11, 6465-6474, doi: 10.5194/acp-11-
598 6465-2011, 2011.
- 599 Nolte, C. G., Schauer, J. J., Cass, G. R., and Simoneit, B. R. T.: Highly polar organic
600 compounds present in wood smoke and in the ambient atmosphere, *Environ. Sci.*
601 *Technol.*, 35, 1912-1919, doi: 10.1021/es001420r, 2001.
- 602 O'Neill, E. M., Kawam, A. Z., Van Ry, D. A., and Hinrichs, R. Z.: Ozonolysis of
603 surface-adsorbed methoxyphenols: kinetics of aromatic ring cleavage vs. alkene
604 side-chain oxidation, *Atmos. Chem. Phys.*, 14, 47-60, doi: 10.5194/acp-14-47-
605 2014, 2014.
- 606 Odum, J. R., Hoffmann, T., Bowman, F., Collins, D., Flagan, R. C., and Seinfeld, J. H.:
607 Gas/particle partitioning and secondary organic aerosol yields, *Environ. Sci.*
608 *Technol.*, 30, 2580-2585, doi: 10.1021/es950943+, 1996.
- 609 Ofner, J., Krueger, H. U., Grothe, H., Schmitt-Kopplin, P., Whitmore, K., and Zetzsch,
610 C.: Physico-chemical characterization of SOA derived from catechol and guaiacol
611 - a model substance for the aromatic fraction of atmospheric HULIS, *Atmos. Chem.*
612 *Phys.*, 11, 1-15, doi: 10.5194/acp-11-1-2011, 2011.
- 613 Park, J.-H., Ivanov, A. V., and Molina, M. J.: Effect of relative humidity on OH uptake
614 by surfaces of atmospheric importance, *J. Phys. Chem. A*, 112, 6968-6977, doi:
615 10.1021/jp8012317, 2008.
- 616 Riva, M., Tomaz, So, Cui, T., Lin, Y. H., Perraudin, E., Gold, A., Stone, E. A., Villenave,
617 E., and Surratt, J. D.: Evidence for an unrecognized secondary anthropogenic
618 source of organosulfates and sulfonates: Gas-phase oxidation of polycyclic
619 aromatic hydrocarbons in the presence of sulfate aerosol, *Environ. Sci. Technol.*,
620 49, 6654-6664, doi: 10.1021/acs.est.5b00836, 2015.
- 621 Sarrafzadeh, M., Wildt, J., Pullinen, I., Springer, M., Kleist, E., Tillmann, R., Schmitt,
622 S. H., Wu, C., Mentel, T. F., Zhao, D., Hastie, D. R., and Kiendler-Scharr, A.:
623 Impact of NO_x and OH on secondary organic aerosol formation from beta-pinene
624 photooxidation, *Atmos. Chem. Phys.*, 16, 11237-11248, doi: 10.5194/acp-16-



- 625 11237-2016, 2016.
- 626 Sato, K., Takami, A., Iozaki, T., Hikida, T., Shimono, A., and Imamura, T.: Mass
627 spectrometric study of secondary organic aerosol formed from the photo-oxidation
628 of aromatic hydrocarbons, *Atmos. Environ.*, 44, 1080-1087, doi:
629 10.1016/j.atmosenv.2009.12.013, 2010.
- 630 Schauer, J. J., Kleeman, M. J., Cass, G. R., and Simoneit, B. R. T.: Measurement of
631 emissions from air pollution sources. 3. C-1-C-29 organic compounds from
632 fireplace combustion of wood, *Environ. Sci. Technol.*, 35, 1716-1728, doi:
633 10.1021/es001331e, 2001.
- 634 Simoneit, B. R. T., Rogge, W. F., Mazurek, M. A., Standley, L. J., Hildemann, L. M.,
635 and Cass, G. R.: Lignin pyrolysis products, lignans, and resin acid as specific
636 tracers of plant classes in emissions from biomass combustion, *Environ. Sci.
637 Technol.*, 27, 2533-2541, doi: 10.1021/es00048a034, 1993.
- 638 Sun, Y. L., Zhang, Q., Anastasio, C., and Sun, J.: Insights into secondary organic aerosol
639 formed via aqueous-phase reactions of phenolic compounds based on high
640 resolution mass spectrometry, *Atmos. Chem. Phys.*, 10, 4809-4822, doi:
641 10.5194/acp-10-4809-2010, 2010.
- 642 Takekawa, H., Minoura, H., and Yamazaki, S.: Temperature dependence of secondary
643 organic aerosol formation by photo-oxidation of hydrocarbons, *Atmos. Environ.*,
644 37, 3413-3424, doi: 10.1016/s1352-2310(03)00359-5, 2003.
- 645 Ulbrich, I. M., Canagaratna, M. R., Zhang, Q., Worsnop, D. R., and Jimenez, J. L.:
646 Interpretation of organic components from Positive Matrix Factorization of
647 aerosol mass spectrometric data, *Atmos. Chem. Phys.*, 9, 2891-2918, doi:
648 10.5194/acp-9-2891-2009, 2009.
- 649 Weis, D. D., and Ewing, G. E.: Water content and morphology of sodium chloride
650 aerosol particles, *J. Geophys. Res.-Atmos.*, 104, 21275-21285, doi:
651 10.1029/1999jd900286, 1999.
- 652 Xu, L., Middlebrook, A. M., Liao, J., de Gouw, J. A., Guo, H., Weber, R. J., Nenes, A.,
653 Lopez-Hilfiker, F. D., Lee, B. H., Thornton, J. A., Brock, C. A., Neuman, J. A.,
654 Nowak, J. B., Pollack, I. B., Welti, A., Graus, M., Warneke, C., and Ng, N. L.:
655 Enhanced formation of isoprene-derived organic aerosol in sulfur-rich power plant
656 plumes during Southeast Nexus, *J. Geophys. Res.-Atmos.*, 121, 11137-11153, doi:
657 10.1002/2016jd025156, 2016.
- 658 Yang, B., Zhang, H., Wang, Y., Zhang, P., Shu, J., Sun, W., and Ma, P.: Experimental
659 and theoretical studies on gas-phase reactions of NO₃ radicals with three
660 methoxyphenols: Guaiacol, creosol, and syringol, *Atmos. Environ.*, 125, 243-251,
661 doi: 10.1016/j.atmosenv.2015.11.028, 2016.
- 662 Ye, J., Abbatt, J. P. D., and Chan, A. W. H.: Novel pathway of SO₂ oxidation in the
663 atmosphere: reactions with monoterpene ozonolysis intermediates and secondary
664 organic aerosol, *Atmos. Chem. Phys.*, 18, 5549-5565, doi: 10.5194/acp-18-5549-
665 2018, 2018.
- 666 Yee, L. D., Kautzman, K. E., Loza, C. L., Schilling, K. A., Coggon, M. M., Chhabra, P.



667 S., Chan, M. N., Chan, A. W. H., Hersey, S. P., Crouse, J. D., Wennberg, P. O.,
668 Flagan, R. C., and Seinfeld, J. H.: Secondary organic aerosol formation from
669 biomass burning intermediates: phenol and methoxyphenols, Atmos. Chem. Phys.,
670 13, 8019-8043, doi: 10.5194/acp-13-8019-2013, 2013.



671 **Table 1.** Experimental conditions and results for guaiacol photooxidation in the presence

672 NO_x .

Expt.	$[\text{Guaiacol}]_0$ ($\mu\text{g m}^{-3}$)	$\Delta[\text{Guaiacol}]$ ($\mu\text{g m}^{-3}$) ^a	$[\text{NO}_x]_0$ (ppb)	$[\text{NO}]_0$ (ppb)	RH (%)	T (K)	M_0 ($\mu\text{g m}^{-3}$) ^b	Yield (%)
1	136.83	112.34	25.1	13.2	39	302	10.63	9.46
2	309.06	282.33	52.7	34.4	38	302	34.72	12.30
3	375.19	335.94	58.3	44.5	40	302	63.62	18.94
4	718.49	613.25	116.7	98.5	38	302	130.19	21.23
5	1321.25	1116.20	209.2	184.1	39	302	256.88	23.01
6	1470.66	1175.03	248	200	38	302	297.65	25.33
7	2197.36	1664.29	335	286	38	302	438.82	26.37

673 ^a The consumed guaiacol concentration at the end of each experiment.

674 ^b M_0 is the mass concentration of SOA.



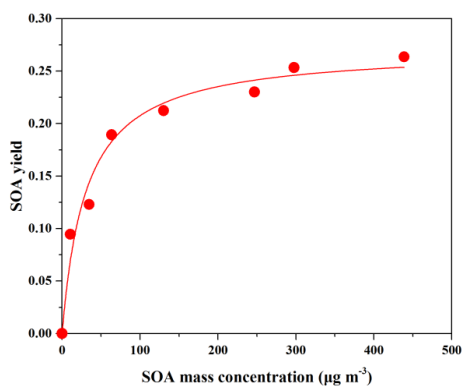
675 **Table 2.** Experimental conditions and results for guaiacol photooxidation in the presence of seed particles and SO₂.

Expt.	[Guaiacol] ₀ ($\mu\text{g m}^{-3}$)	$\Delta[\text{Guaiacol}]$ ($\mu\text{g m}^{-3}$) ^a	Seed	[SO ₂] ₀ (ppb)	[NO _x] ₀ (ppb)	[NO] ₀ (ppb)	RH (%)	T (K)	N _s (m^{-3}) ^b	D _s (nm) ^c	C _{seed} ($\mu\text{g m}^{-3}$) ^d	C _{sulfate} ($\mu\text{g m}^{-3}$) ^e	S ₀ ($\mu\text{m}^2 \text{cm}^{-3}$) ^f	S _r ($\mu\text{m}^2 \text{cm}^{-3}$) ^g	M ₀ ($\mu\text{g m}^{-3}$) ^h	Yield (%)	OSC ⁱ
1	375.19	335.94	–	–	58.3	44.5	40	302	–	–	–	–	–	1.25×10^3	63.62	18.94	0.11
2	363.53	332.79	–	33	54.5	37.4	38	302	–	–	–	7.42	–	1.68×10^3	71.88	21.60	0.14
3	370.12	335.58	–	56	57.3	41.8	38	302	–	–	–	17.89	–	2.04×10^3	78.59	23.42	0.18
4	379.05	346.03	NaCl	–	58.8	40.7	39	302	10700	56	15.63	–	2.69×10^2	1.47×10^3	84.91	24.54	0.29
5	378.44	339.34	NaCl	30	57.4	41.9	38	302	11300	58	13.84	7.51	2.64×10^2	2.32×10^3	90.89	26.78	0.30
6	380.77	340.15	NaCl	54	60.1	46.1	39	301	11200	56	14.28	16.67	2.81×10^2	2.91×10^3	98.86	29.06	0.33
7	373.57	340.86	(NH ₄) ₂ SO ₄	–	58.3	42.6	39	302	10400	53	15.45	–	2.75×10^2	1.53×10^3	79.44	23.31	0.20
8	376.26	343.19	(NH ₄) ₂ SO ₄	33	56.8	38.9	38	302	10100	53	14.38	7.84	2.80×10^2	2.57×10^3	84.35	24.58	0.22
9	381.33	341.01	(NH ₄) ₂ SO ₄	54	57.8	39.2	38	303	10700	51	14.90	17.25	2.82×10^2	3.10×10^3	89.92	26.37	0.23

676 ^a The consumed guaiacol concentration at the end of each experiment. ^b N_s is the initial seed number. ^c D_s is the average diameter of seed particles.

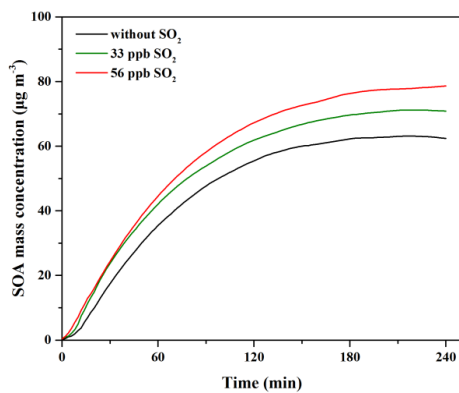
677 ^d C_{seed} is the initial concentration of seed. ^e C_{sulfate} is the sulfate concentration formed by SO₂ oxidation. ^f The initial surface area of seed particles.

678 ^g The final surface area of aerosol particles (seed + organic aerosol), measured by SMPS. ^h M₀ is the mass concentration of SOA. ⁱ OSC is the
 679 average oxidation state of carbon of SOA.



680

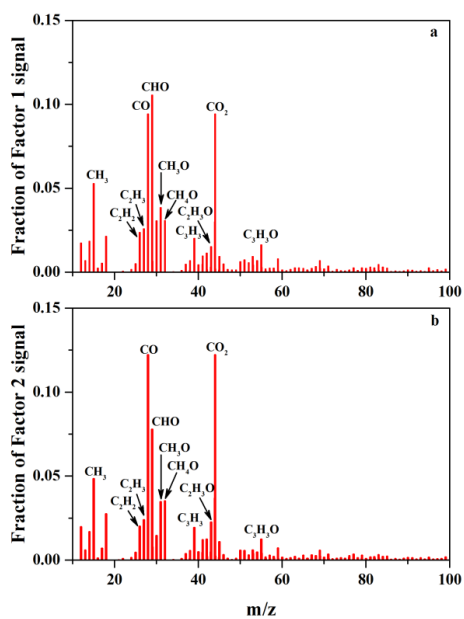
681 **Figure 1.** SOA yield as a function of SOA mass concentration (M_0) for guaiacol
682 photooxidation in the presence of NO_x at different guaiacol concentrations. The solid
683 lines was fit to the experimental data using a one-product model. Values of α and $K_{\text{om},i}$
684 used to generate the solid line were (0.27 ± 0.01) and (0.033 ± 0.008) in this work.



685

686 **Figure 2.** Time-dependent growth curves of SOA mass concentration for guaiacol

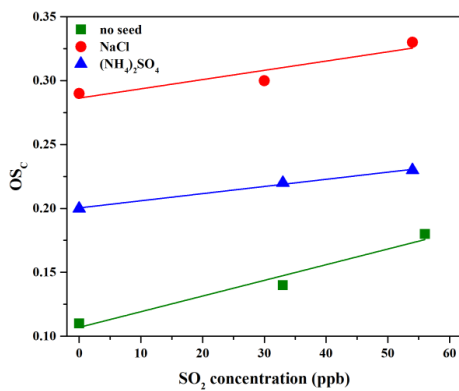
687 photooxidation at different SO₂ levels (Expts. 1–3 in Table 2).



688

689 **Figure 3.** Mass spectra of Factor 1 (a) and Factor 2 (b) for the formed SOA identified

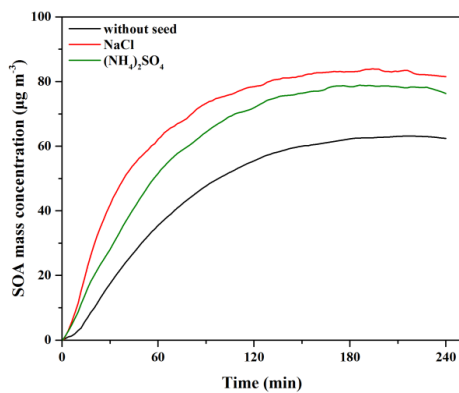
690 by applying PMF analysis to the AMS data.



691

692 **Figure 4.** OS_c of SOA formed in the presence of various seed particles as a function of

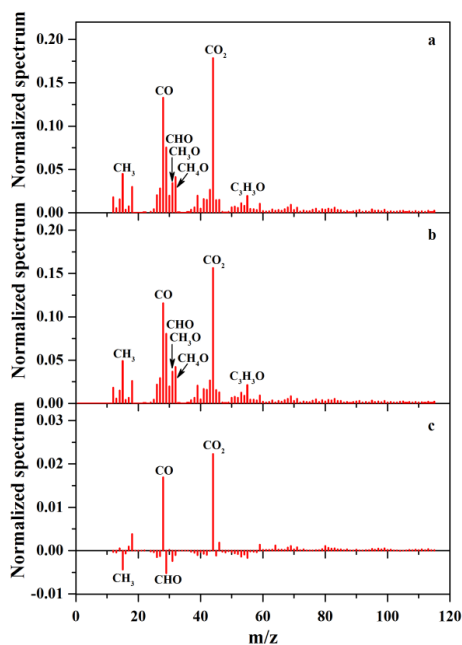
693 SO₂ concentration.



694

695 **Figure 5.** Time-dependent growth curves of SOA mass concentration for guaiacol

696 photooxidation in the presence of inorganic seed particles (Expts. 1, 4 and 7 in Table 2).

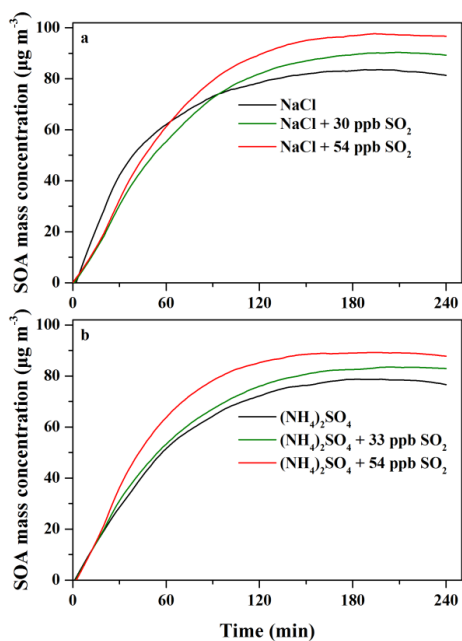


697

698 **Figure 6.** Mass spectra of SOA with NaCl (a) and (NH₄)₂SO₄ (b) as seed particles

699 obtained by HR-ToF-AMS, as well as their difference mass spectrum (c) obtained by a

700 minus b.



701

702 **Figure 7.** Time-dependent growth curves of SOA mass concentration for guaiacol

703 photooxidation in the presence of SO_2 and inorganic seed particles (a, NaCl; b,

704 $(\text{NH}_4)_2\text{SO}_4$) (Expts. 4–9 in Table 2).